Luminescence dating of irrigation systems: application to a qanat in Aragon, Spain

Supplementary Material

1. Site Location

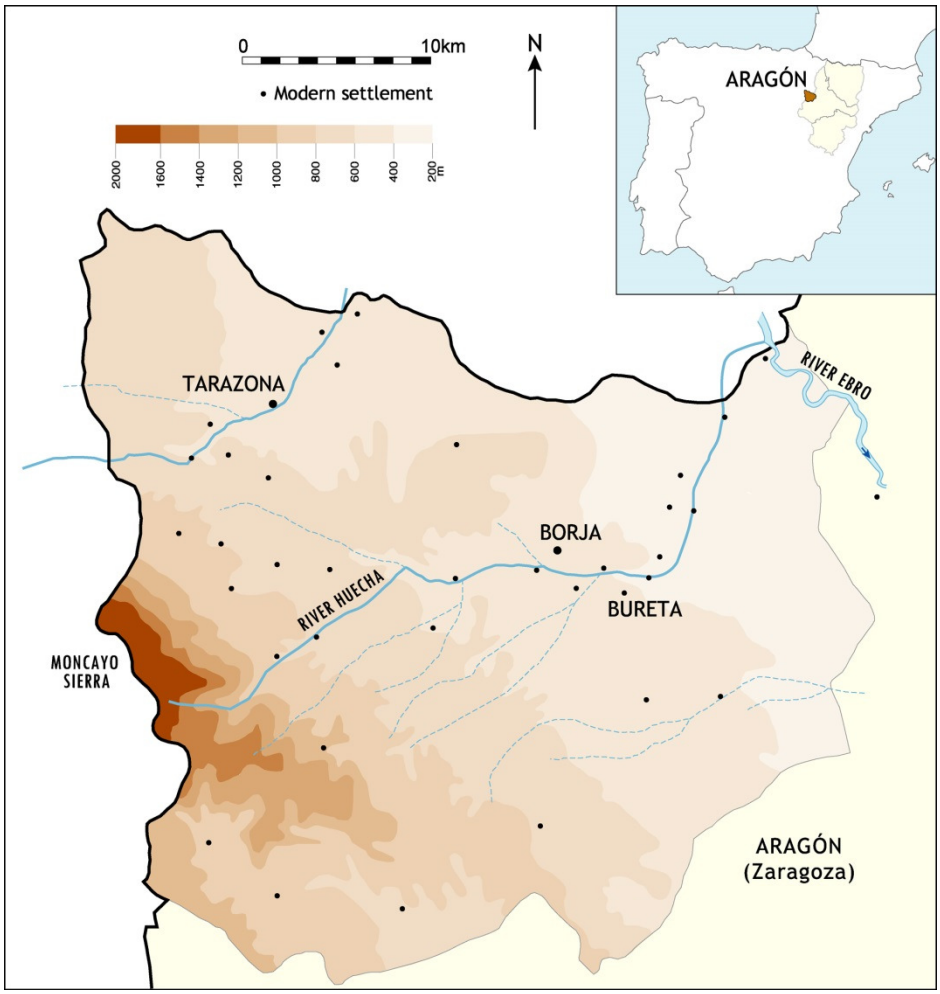

Figure SM1
Location map for Bureta in the province of Zaragoza (Aragón), north-east Spain. The village lies immediately south of the stream bed of the River Huecha

2. Lithology

The sections excavated and recorded during the second phase of fieldwork, in mounds S2 (391-3) and S3 (391-4), shown in Fig. SM2 and their lithological descriptions are summarised below in Table SM1a,b for each section.

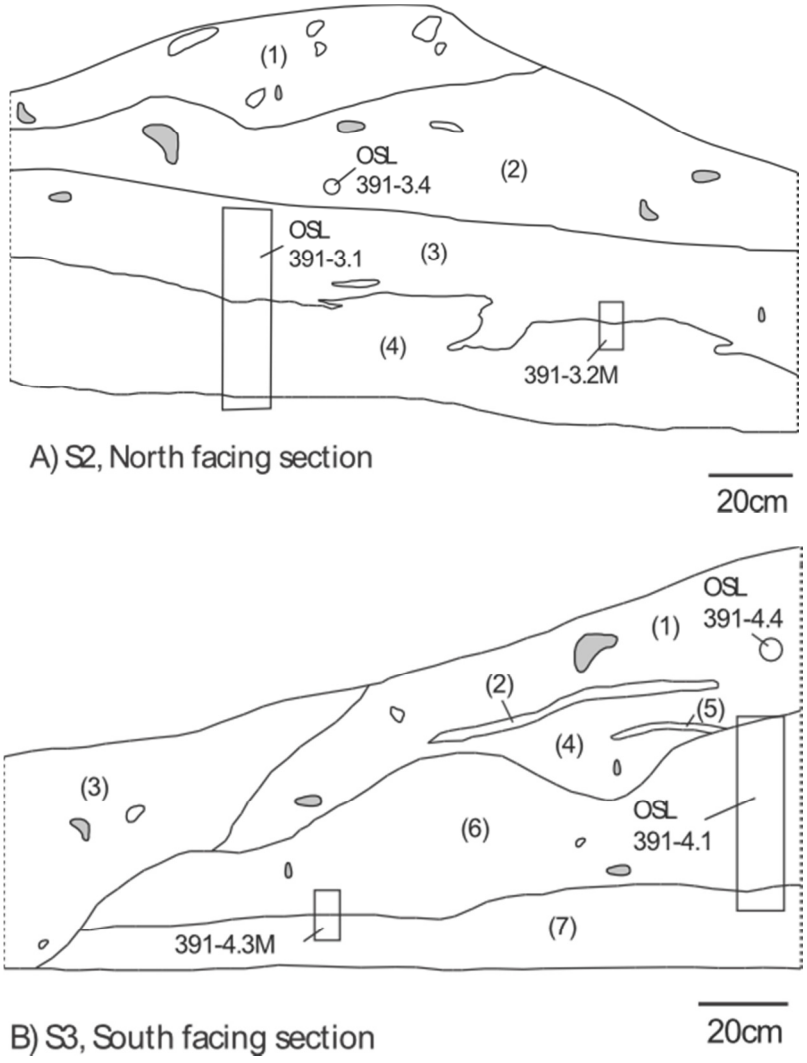

Figure SM2.

Sections recorded for excavations of A) mound S2 (391-3) and B) mound S3 (391-4), where a description of the numbered stratigraphic units (SU) is summarised in Tables SM1a and SM1b respectively. The rectangular outlines indicate the position of the blocks extracted for OSL and micromorphological analysis.

Table SM1a. Sediment descriptions of north-facing section of S2.

Srat. Unit	Deposit	Munsell colour (wet)	Sediment description
(1)	Upcast	10YR 4/3	Silty loam, loose, poorly sorted, frequent clay aggregates and sandstone and mudstone inclusions, pebble size, sub-angular in shape, randomly orientated, frequent fine roots, sharp boundary.
(2)	Upcast	10YR 5/3	Silty clay, loose, moderately sorted, frequent clay aggregates, granular in size, sub-angular shape, Fe mottling, occasional fine roots, sharp boundary.
(3)	Upcast	10YR 5/4	Silty clay, compact, poorly sorted, frequent clay and mudstone aggregates, sub-angular in shape, randomly orientated, sharp undulating boundary.
(4)	Palaeosol	7.5YR 6/4	Silty sand, compact, moderately sorted, occasional fine roots.

Table SM1b. Sediment descriptions of south-facing section of S3.

Srat. Unit	Deposit	Munsell colour (wet)	Sediment description
(1)	Upcast	10YR 6/3	Silty clay, loose, moderately sorted, clay aggregates of pebble-granular size, inclusions sub-angular in shape, frequent fine roots, sharp boundary.
(2	Humic layer	10YR 3/1	Silty clay, loose, moderately sorted, frequent fine roots, Fe translocation, sharp boundary.
(3)	Upcast	10YR 6/4	Sandy silt, loose, moderately sorted, occasional clay aggregates, inclusions sub-angular in shape, frequent large roots, sharp boundary.
(4)	Upcast	7.5YR 6/4	Clay, loose, moderately sorted, frequent clay aggregates, sub-angular and platy in shape, sharp undulating boundary.
(5)	Humic layer	2.5YR 3/1	Silt, loose, well sorted, frequent charcoal inclusions, sharp boundary.
(6)	Upcast	10YR 5/4	Silty clay, compact, well sorted, occasional mudstone inclusions, sub-angular in shape, sharp boundary.
(7)	Upcast	10YR 5/3	Silty clay, compact, well sorted, frequent clay aggregates of pebble size.

2. Micromorphology

2.1. Examination thin section 391-3.2M, shaft mound S2

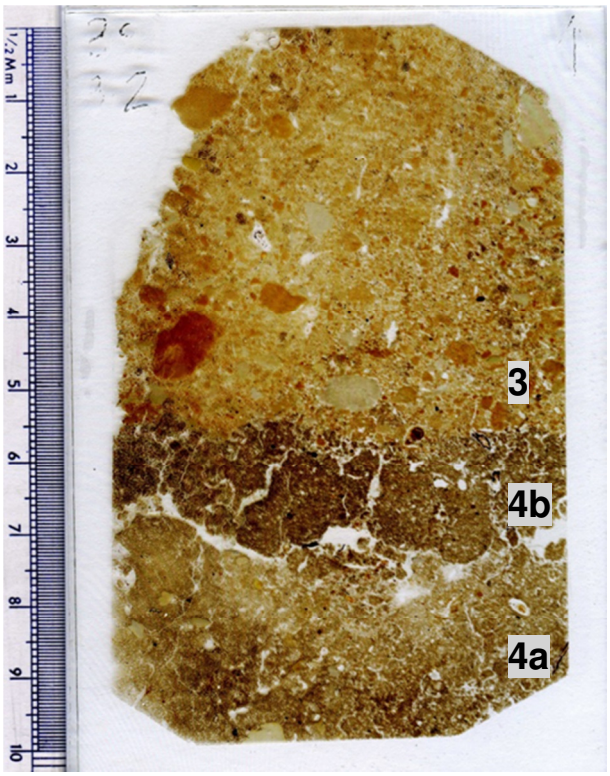

Figure SM3a.
Scanned image (300 dpi) of thin section 391-3.2M (approx. size 100x65 mm). The numbers correspond to SU numbers shown in section drawing (Fig. SM2a)

Deposit 1 is a compact silty clay loam with weak subangular blocky peds with vughs, planes and chamber voids. Occasional traces of bioturbation are also present. Inorganic inclusions include biotite, epidote and fragments of schist. The most abundant mineral inclusion is quartz with 50% of grains showing first stages of weathering and are spherical in shape and sub-rounded. Fragments of charcoal, shell and occasional pollen grains are present.

Deposit 2 has the same texture, sorting, microsctructure and inclusions but shows more evidence for bioturbation with F_e coatings and Magnanese (M_g) inclusions within voids. The boundary between deposit 2 and 3 appears to be abrupt and undulating.

Deposit 3 is a crumbly silty clay with a granular open structure with occasional F_e mottling around voids. The deposit contains plagioclase, K-feldspars and quartz with some evidence for weathering and transport resulting in a spherical subrounded to rounded shape in mineral grains. 50% of the SU consists of large clay clods. Two deposits were analysed from the upcast from S3.

3. 2.2. Examination thin section 391-4.3M, shaft mound S3

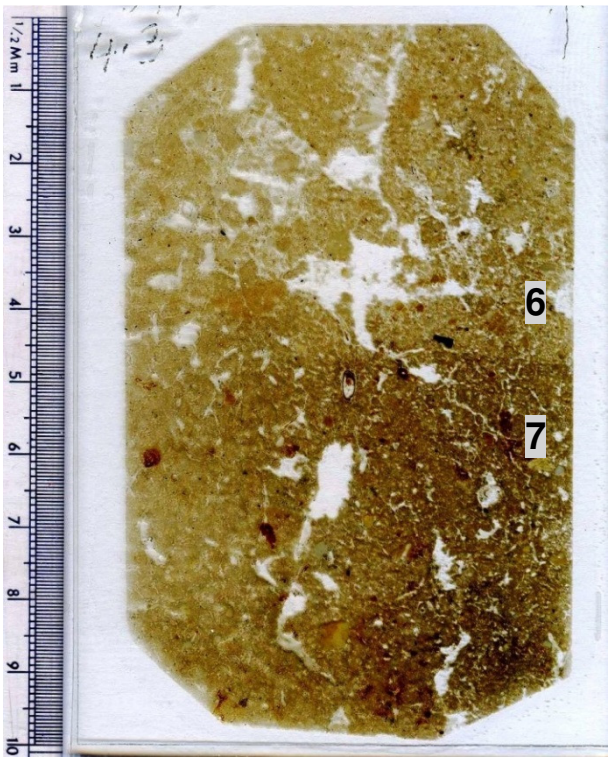

Figure SM3b
Scanned image (300 dpi) of thin section 391-4.3M (approx. size 100x65 mm). Numbers correspond to SU numbers shown in section drawing (Fig. SM2b)

Deposit 4 is characterised as unsorted sandy clay with massive microsctructure and irregular blocks with occasional planes and vughy voids. There is frequent evidence for biotubation caused by root action. The main inclusions include muscovite, K-feldspar and 25-30% quartz inclusions. Degraded roots, charcoal fragments and shell are present within the sediments. The boundary between deposit 4 and 5 is flat and sharp.

Deposit 5 is a strongly bioturbated sandy clay loam with a crumb microstructure, and many vughs, planes and channel voids. Inclusions include moderately weathered quartz (10-15% frequency); other inclusions include plagioclase, feldspar, muscovite, biotite and basalt fragments and occasional fragments of organic remains such as degraded roots, charcoal and shell.

2.3. Cross polarised images of thin sections

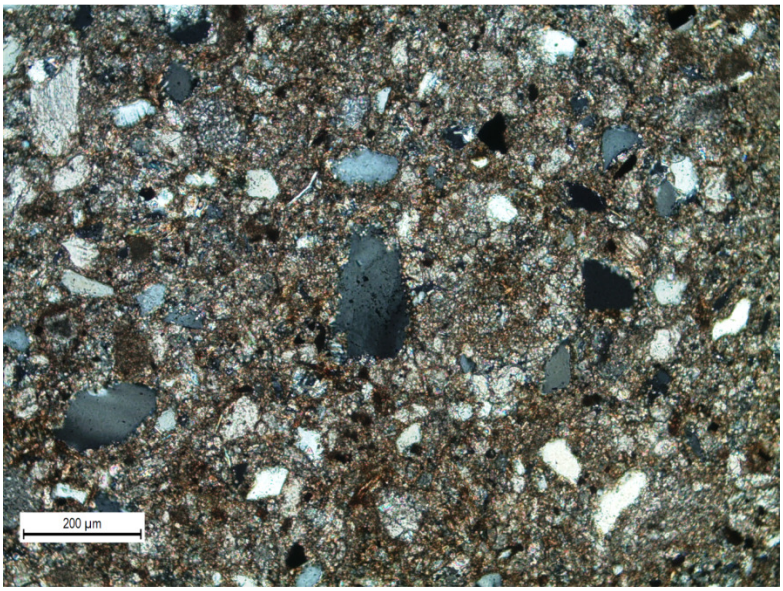

Figure SM3c.
Rounded quartz and calcite rich fine sand in clod. Evidence for enaulic distribution of fine material partially filling spaces between coarse grains. XPL (x10). Slide 391-3.2M (S2), deposit 3.

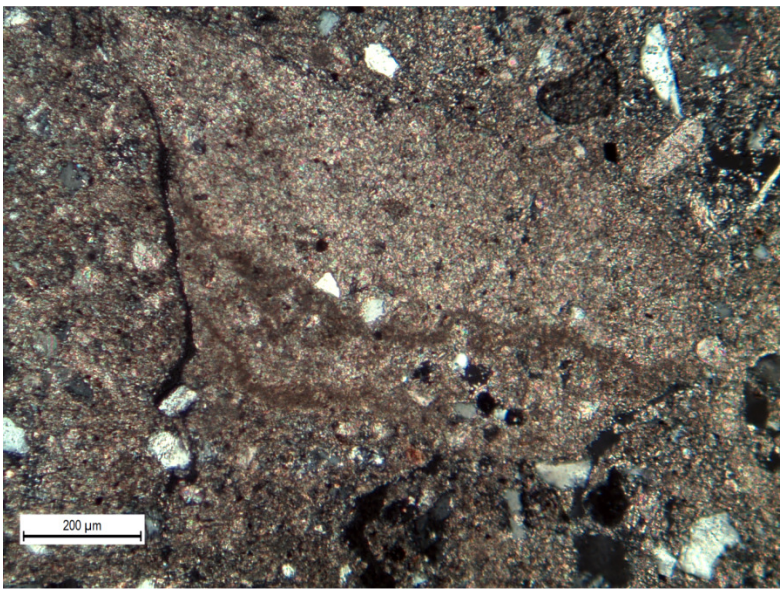

Figure SM3d.
Micritic calcareous deposit: fine-grained clod with clay laminations. XPL (x10) Thin section 319.4.3M, SU 7.

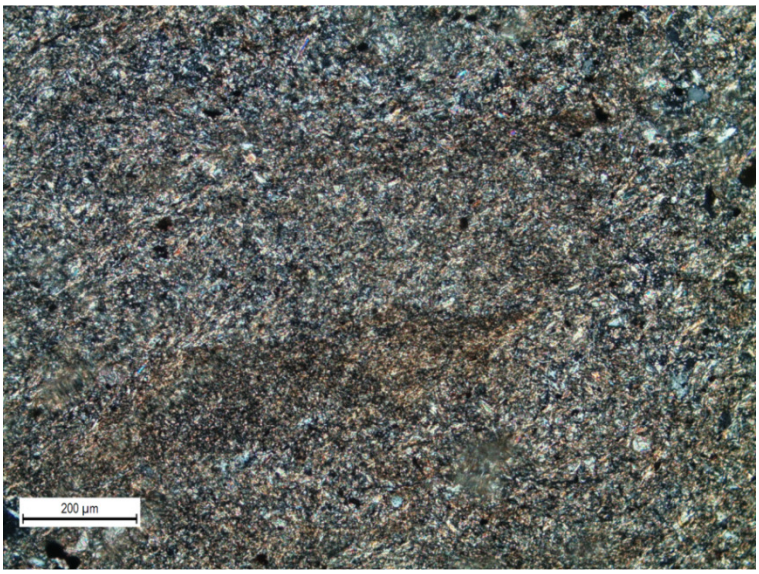

Figure SM3e.
Micritic calcareous fine-grained clod showing poorly laminated clay particles and elongated calcite minerals with parallel and random distribution and orientation. XPL (x10). Slide 391-3.2M (S2), SU 3.

Table SM2a. Thin section analysis: deposit characteristics and frequency of post-depositional features:

Thin section	Shaft	Srat. Unit	Sediment description	Related distribution	Microstructure	Post-depositional processes
391-4.3M	S3	5	Bioturbated moderately sorted sandy clay loam	Loose porphyric	Crumb and irregular blocky peds and vughs, planes and channel voids.	Bioturbation +++
391-4.3M	S3	4	Unsorted sandy clay	Loose porphyric	Massive structure and irregular blocks, occasional planes and vughy voids. Elongated calcite crystals orientated parallel to each other.	Bioturbation++ C_aCO_2 coating voids +
391-3.2M	S2	3	Crumbly moderately sorted silty clay	Close pophyric and enaulic	Granular open structure	Fe mottling + C_aCO_2 coating voids +
391-3.2M	S2	2	Compact moderately sorted silty clay loam	Close pophyric	Weak subangular block peds, with planes, vughs and channels.	Bioturbation ++ Fe coating voids and mottling + Manganese +
391-3.2M	S2	1	Compact moderately sorted silty clay loam	Close pophyric	Weak subangular block peds with vughs, planes and chambers	Bioturbation +

+ Occasional, ++ Frequent, +++ Abundant

Table SM2b. Thin section analysis: description of sediment aggregates

Srat. Unit	Quartz %	Level of weathering	Grain size range (min-max)	Other mineral/rock inclusions	Organic inclusions	Clay aggregates %	Clay aggregate size
5	10-15%	1-2	<10-450µm	Plagioclase feldspar, muscovite, biotite, basalt.	Degraded root material, charcoal fragments and shell fragments	10%	600µm-1cm
4	25-30%	1	<10-400µm	Muscovite, k-feldspar	Degraded roots, charcoal fragments, pollen grains, shell fragments	15%	600-µm 0.6mm
3	25-30%	1	<10-400µm	Plagioclase, k-feldspar	Degraded roots, amorphous organic material, charcoal, shell fragments	50%	600µm-1cm
2	40-45%	1	<10-250µm	K- feldspar, biotite, epidote	Degraded roots, charcoal fragments, bone fragment.	5%	600-1000µm
1	40-45%	1	<10-450µm	Biotite, epidote, schist	Amorphous organic material, degraded roots, pollen grains, shell fragments and charcoal fragments.	15%	600-1cm

3. Luminescence

3.1 Sample preparation

Once in the laboratory, the sampled blocks were partly encased in rigid plaster to maintain structural integrity of the blocks during sub-sampling of the sediment. After removal of surface material (used for dose rate assessment) to a depth of at least 10 mm, sediment was excavated from slots of ~12 mm (vertical) depth. From this material, coarse quartz grains were extracted following the procedures developed for the quartz inclusion technique (Aitken, 1985) and all sample preparation was performed under subdued red lighting conditions. The 150-200 µm and 200-355 µm sieved fractions were treated in 15% HCl to remove carbonates, followed by etching in HF (40%, 45 mins), and finally immersed in HCl (40%) for 45 mins to remove fluoride precipitates, using appropriate washing procedures at each stage. The HF etched material was finally re-sieved, to remove grains smaller than the lower diameter of the above sieved ranges. The 200-355 µm was the preferred fraction for OSL measurements to gain higher OSL signal intensity and where there was insufficient material the smaller 150-200 µm fraction was used. Small aliquots of HF etched grains were deposited using a dental spatula onto stainless steel discs that had been lightly sprayed with silicone oil through a mask of ~6 mm dia., taking care to disperse the grains to avoid clustering. Typically aliquots contained ~50 and ~100 grains for palaeosol and upcast samples respectively. Before use all discs had been checked for the absence of background signal interference by applying a beta dose of ca 5 Gy, a preheat (220°C) and measuring the OSL response.

3.2 Instrumentation

The OSL was stimulated using a blue LED array (470 nm; ~35 mW cm^{-2}) mounted in the Risø TL-DA-12 semi-automated reader (Risø National Laboratory, Denmark) and detected after passing through a Hoya U340 filter (7.5 mm). The decay curve (Fig. SM3a) was recorded for 50 s while maintaining a sample temperature of 125 ºC during stimulation to prevent retrapping of charge by traps associated with the 110 °C TL peak; the photon counter interval was set to 200 ms.

Following completion of the SAR measurement procedure for each aliquot, the spatial distribution of OSL from grains within the aliquots was measured using a scanner (Bailiff and

Mikhailik, 2003) that mapped the distribution of OSL from the scanned area (10 mm x 10 mm) containing 1600 measurement points (Fig. SM4b). The OSL map obtained was analysed by fitting a contour plot to the data and visually assessing the number of regions with bright emission and comparing this distribution with a photographic image of the disc obtained after scanning had been completed. The digital record of OSL intensity enables integration of the OSL signal within delineated regions to allow comparison of relative intensity, but this procedure has yet to be automated within image processing software.

The primary calibration of the beta source in the luminescence reader was originally performed with 90-150 μm and 150-200 μm diameter quartz grains that had been gamma irradiated at a Secondary Standards Laboratory (Göksu et al., 1995), and subsequently checked periodically using gamma photon irradiated quartz. Armitage and Bailey (2005) have observed experimentally, using a similar Risø reader and irradiation geometry, an absence of significant variation of the source beta dose rate with grain size (within the limits of experimental uncertainty), tested with grains between ca 65 μm and 250 μm diameter. We have also observed this absence of a significant grain size dependence for larger grains when applying our calibration absorbed dose determinations with gamma irradiated quartz (180-250 μm dia.) circulated as part of the Risø Laboratory intercomparison and similar predictions have been obtained from radiation transport simulations (MCNP 5) for the source geometry in our reader, with modelled grain sizes between 120 and 350 μm diameter.

3.3. Equivalent dose

The equivalent dose, D_e, was determined using a single aliquot regeneration (SAR) OSL procedure, similar to that described by Murray and Wintle (2000; 2003), but where the corrections for sensitivity change and thermal transfer are handled differently (Table SM3a). The test dose in the SAR protocol was replaced by a monitor dose comparable to the estimated natural dose; three levels of regenerative dose were applied to provide a range extending from half to two times the estimated natural dose. A second preheat and the following OSL decay curve measurement (referred to as a pre-heat monitor, PHM) were included in the sequence to examine the OSL signal arising from thermal transfer, and also to define the background signal (referred to as PBG). During the first preheat for this pair of OSL measurements, the TL was recorded to monitor changes in TL sensitivity. The OSL signal, used to construct the dose response plots, corresponds to the counts recorded during the initial 800 ms of the OSL decay curve (including the background, PHM). The early background (EBG) subtraction procedure (Ballarini et al, 2007; Cunningham and Wallinga, 2010) was also applied using signal integration intervals of 0-800 ms and 800-1600 ms for signal and background respectively. Agreement within experimental errors of the D_e values calculated using EBG and PBG subtraction was used to check for the absence of intrusive medium and slow decay components (Li and Li, 2006; Steffen et al, 2009) where the OSL signals were sufficiently strong.

Tests for meeting the criteria for satisfactory luminescence characteristics (Wintle and Murray, 2006) were applied and aliquots with recycling and IR depletion ratios deviating more than 10% from unity were excluded from further analysis. No cases of non-intersection of the natural signal with the dose response curve were observed.

Linear dose response curves were fitted to the sensitivity corrected OSL signals by applying a Monte Carlo (MC) simulation combined with a least squares algorithm incorporated in a Microsoft Excel sheet employing Solver and MCSimSolver (Barreto and Howland, 2006) add-ins. For each stage of the Monte Carlo simulation, the OSL signal intensity was drawn from a normal distribution with a relative standard deviation derived from the (Poisson) uncertainty in the net integrated counts. The standard deviation of the distribution of D_e values calculated by the simulation (50 cycles) was used as the estimate of uncertainty in D_e. The analysis of D_e distributions included the use of the central dose (CDM), minimum dose (MDM) and finite mixture statistical models (FMM), seeking the maximum and minimum values respectively of the log likelihood and the Bayesian information criterion, developed by Galbraith (2005).

The dose recovery experiment (Wintle and Murray 2006) was performed using one value of applied dose, D_a, selected to be approximately equivalent to the natural dose, and three preheat temperatures within the range 180-240 °C. The trapped charge was depleted at room temperature (RT) using the blue LED source and, following storage for 10 ks to deplete phototransferred charge in the traps associated with the 110 °C TL peak, any residual charge in the traps used for dosimetry was removed by a further OSL measurement at RT. The experimentally determined value of the equivalent dose, D_e, was obtained using the SAR procedure and the average values of the ratio D_e/D_a are given in Table SM3b.

3.4. Dose rate assessment

3.4.1 High resolution gamma ray spectrometry

The average specific activities (Bq kg^{-1}) of ^{238}U, ^{232}Th and ^{40}K in the sample matrix were measured using a high resolution γ ray spectrometer configured with shielding for low background (Canberra high purity germanium coaxial detector type GR2018 of 20% efficiency and with a Be window). The spectrometer was calibrated using silica-rich sands containing lithogenic radionuclides of certified concentrations (New Brunswick Laboratories, USA and NCS DC73374 standard supplied by LGC Promochem). The samples (~25 g, dried, but without any further treatment) were placed in sealed containers and measured after storage of 3 days and after one month.

The measured specific activities of the sediment samples are given in Table SM3.4. The ^{210}Pb: ^{226}Ra activity ratios obtained from the γ spectrometry measurements indicate longer term *in situ* loss of ^{222}Rn gas in the case of some of the samples (samples 1 and 4). Fortunately a high proportion (ca 80%) of the total dose rate within the sediment is delivered by ^{40}K and the Th series, and the average contributions by ^{238}U to the beta and gamma dose rates are 20% and 27% respectively. In the case of sample with a 50% loss of radon and progeny within the horizon the total dose rate is calculated to reduce by ~5%.

3.4.2 β thermoluminescence dosimetry

The β-TLD technique employs a single 10 mm diameter detector to measure the average β dose rate from sources distributed within the sample volume (~1 cm^3), and a calibration factor is applied to the measured external dose rate to obtain the infinite medium dose rate. The measurements were performed with typically five separately drawn aliquots of sediment (dried, but without any further treatment) to examine the extent of variation in beta dose rate; the sample containers were not sealed to retain radon during the measurement period.

3.4.3 Gamma and cosmic dose rate model

A spreadsheet-based multiple-layer gamma dose rate model (Bailiff et al., 2014), developed initially for application in coastal contexts (Bailiff and Tooley, 2000) and employing geometry coefficients calculated by Løvborg and given in Aitken (1985; Appendix H), was used to calculate the gamma dose rate at a selected depth (the sample position) in a layer of specified concentrations of lithogenic radionuclides (U, Th and K) that are assumed to be uniformly dispersed in each of up to five semi-infinite layers, each of specified thickness. The model includes two layers above and two layers below the designated sample layer, where the thickness of each layer can be varied from ca 1 cm upwards; the dose rate is also adjusted for the moisture content specified in each layer. The model was applied to calculate the gamma dose rate at the sample position in the 'static' configuration, taking into account sediment strata of differing radionuclide content within ~50 cm of the sample position. The cosmic dose rate was calculated at the sample position using Prescott and Hutton's (1988) empirical depth-dose data.

To obtain an estimate of the time-averaged dose rate within the sampled volume since initial burial (apart from the adjustments made to account for moisture content), a simple staged dynamic model was applied. Following initial burial, the deposits lying beneath the sampled volume provide a half infinite-medium for the gamma dose rate and thereafter the gamma dose rate increases during the development of overburden until its depth is sufficient to obtain an infinite medium dose rate (~50% achieved at 5 cm and ~95% at 20 cm for a sediment with 25%

moisture content). In the case of aggradation of the palaeosol (i.e., below the buried ground surface), an average dose-rate during a specified period of overburden development (based on an estimated rate of aggradation) was calculated. In the case of upcast deposition, the time to obtain an infinite medium gamma dose rate was assumed to be short relative to the full burial period. As the depth of upcast overburden increases there is a counteracting decrease in cosmic dose rate (Prescott and Hutton, 1988).

At relatively shallow depths of overburden – as for the shaft mounds - the variation in cosmic dose rate with depth is dominated by the attenuation of the 'soft' electron component that is removed by a depth of about 60 cm in sediment and the 'hard' muon component persists, reducing at a significantly lower rate with depth. The cosmic dose rate was consequently calculated at each stage of overburden development employing Prescott and Hutton's (1988) empirical depth-dose data.

A time-averaged gamma and cosmic dose rate for the full burial period was calculated, weighting the combined dose rate by the duration assigned to each stage of development of the overburden. For the pilot study the latter were estimated on the basis of the assumed depth of upcast deposited in single operations (construction and maintenance) and the rate of palaeosol aggradation derived from OSL dates calculated using the static dose rate model.

Table SM3a OSL single aliquot regenerative procedure (linear response; 3-point)

Step	Procedure	β dose	Measurement	OSL Signal
1	PH1; OSL		Pre-heat using a selected temp. within the range 180-240 ºC; measure OSL	I_N
2	PH2; OSL		Pre-heat monitor (PHM)	I_{BG}
3	ß1; PH1; OSL	β	1st dose point / Sensitivity Monitor	$I_{\beta 1}$
4	PH2; OSL		PHM	I_{BG}
5	ß2; PH1; OSL	0.5β	2nd dose point	$I_{\beta 2}$
6	PH2; OSL		PHM	I_{BG}
7	ß3; PH1; OSL	β	Sensitivity Monitor	$I_{\beta 3}$
8	PH2; OSL		PHM	I_{BG}
9	ß4; PH1; OSL	2β	3rd dose point	$I_{\beta 4}$
10	PH2; OSL		PHM	I_{BG}
11	ß5; PH1; OSL	β	Sensitivity Monitor	$I_{\beta 5}$
12	PH2; OSL		PHM	I_{BG}
13	ß6; PH1; OSL	0.5β	Repeat ß2/Recycling test	$I_{\beta 6}$
14	PH2; OSL		PHM	I_{BG}
15	ß7; PH1; IRSL;OSL	β	Sensitivity Monitor/Test for IR response	$I_{\beta 7}$
16	PH2; OSL		PHM	I_{BG}
17	ß8; PH1	~3β	ß dose and PH	Scan

Notes

1. The OSL decay curve was measured for 20s with the sample temperature held at 125 ºC during stimulation.
2. The preheat PH1 was performed by heating the aliquot (5 ˚C s^{-1}) to a maximum temperature selected in the range 200-240 ˚C, recording the TL, holding at the maximum temperature for 5s, cooling to RT and then repeating the procedure. The preheat PH2 was performed by heating once to the maximum temperature as in PH1 and holding at that temperature for 10s.
3. ßn represents the administration of a laboratory ß dose in the regenerative sequence, where Steps 3, 7, 11 and 15 correspond to the monitor dose and where Steps 5 (β2) and 9 (β4) correspond to 0.5 times and 2 times the monitor dose respectively. The monitor dose was selected to be approximately equal to the burial dose ($\beta \cong D_e$).
4. The dose response curve was plotted using the OSL signal values, after subtraction of the background signal (I_{BG}), and normalisation to the preceding (except for I_N) sensitivity monitor as in the conventional SAR procedure, producing the following three sets of data pairs: 0, $I_N/I_{\beta 1}$; ß1, $I_{\beta 1}/I_{\beta 1}$; ß2, $I_{\beta 3}/I_{\beta 2}$; ß4, $I_{\beta 4}/I_{\beta 3}$. The recycling ratio was determined by evaluating the expression $(I_{\beta 6}/I_{\beta 5})/(I_{\beta 3}/I_{\beta 2})$; IR depletion was tested by examining the position of $I_{\beta 7}$ relative to the extrapolated trend line fitted to values of the sensitivity monitors, $I_{\beta 1}$, $I_{\beta 3}$, $I_{\beta 5}$ plotted against cumulative dose.
5. For the dose recovery experiment, the trapped charge was depleted at room temperature (RT) using the blue LED source and, following storage for 10 ks to deplete phototransferred charge in the traps associated with the 110 ºC TL peak, any residual charge in the traps used for dosimetry was removed by a further OSL measurement at RT. Following this treatment, the applied dose, D_a, administered, selected to be approximately equivalent to the natural dose, and step 1 in the above procedure then commenced.

Table SM3b Equivalent dose, statistical data

							Grain Count				Statistics			
	Type	Dose recovery $D_e/D_a \pm$ s.e. 200 -240 ph	OD σ_i %	n	Recycling ratio ± s.e.	Total n	1gr	2 gr	3gr	4gr	OD σ_b 1gr %	Wgt Skew c (%crit. val.) 1gr	OD σ_b >1gr %	Wgt Skew c (%crit. val.) >1gr
1.3	UC	0.98±0.05	15	12	0.98±0.04	34	14	13	6	1	42	0.33 (26%)	30	-0.02 (2%)
1.2	UC	0.87±0.06	14	6	1.00±0.07	31	16	13	2		54	1.77 (144%)	23	0.21 (17%)
1.1	UC	0.92±0.08	22	8	0.90±0.06	22	16	3	2	1	20	0.29 (24%)	51	0.49 (25%)
2.3	UC	0.90.±0.04	10	10	1.07.±0.06	25	9	13	1	3	93	-0.30 (18%)	130	0.34 (30%)
2.2	PS	0.93.±0.05	14	11	0.97.±0.06	42	19	13	5	5	73	0.67 (60%)	60	0.31 (31%)
2.2L	PS	-	10	6	1.05.±0.05	32	10	12	9	1	35	-0.16 (10%)	17	0.54 (52%)
2.1	PS	1.01±0.05	5	6	0.96±0.06	22	4*	8	8	2	46(0)*	-0.05 (2%)*	54	0.10 (9%)
3.1.4	UC	0.96±0.05	14	9	1.00±0.03	19	9	6	2	2	56	1.07 (66%)	51	-0.23 (15%)
3.1.3	UC	0.95±0.03	8	7	0.99±0.04	53	29	17	5	2	54	0.55 (60%)	35	-0.64 (63%)
3.1.2	PS	0.97±0.02	6	11	1.02±0.02	40	15	17	6	2	44	0.91 (72%)	16	-1.11 (60%)
3.1.1	PS	1.00±0.04	8	8	0.97±0.05	16	12	3	.	1	29(21)*	0.27 (18%)*	11	0.62 (25%)
4.1.5	UC	0.96±0.27	23	14	0.98±0.06	18	9	4	1	4	91	0.39 (24%)	100	0
4.1.3	UC	0.93±0.03	8	10	1.00±0.03	46	18	9	14	5	72	-0.60 (49%)	88	0.56 (59%)
4.1.2	UC	0.97±0.05	0	6	0.92±0.04	43	18	11	6	10	76	1.00 (86%)	63	0.90 (93%)
4.1.1	UC	0.95±0.05	14	10	0.92±0.04	12	4	5	2	1	14	0.46 (19%)	9	0.18 (10%)

Notes

1. Grain count 1gr, 2gr, 3gr, etc., denotes 1, 2, 3, .. dominant grains in an aliquot as detected using the scanning procedure.
2. OD (col. 13) is the overdispersion calculated using the CDM, including D_e values for all 1gr aliquots.
3. The asterisks denote the effect of removing one outlying D_e value, as discussed in the main text of the paper.

Table SM3c
Specific activities of sediment samples grouped by location.

Sample #	Th	U	K	$^{210}Pb/^{226}Ra$
Bq kg^{-1}	Bq kg^{-1}	Bq kg^{-1}	Bq kg^{-1}	
1.3	30.3±3.0	31.5±1.8	428±7	0.81±0.11
1.2	30.0±3.2	29.5±1.9	451±8	0.74±0.12
1.1	34.6±3.5	47.5±2.2	441±8	0.73±0.08
2.3	33.0±3.1	29.1±1.8	451±7	0.82±0.11
2.2	30.5±3.1	28.5±1.8	418±7	0.86±0.13
2.2L	32.9±3.1	33.3±1.8	463±7	0.71±0.10
2.4	30.9±3.2	29.7±1.9	447±7	0.99±0.16
3.1.4	31.2±3.3	28.8±1.9	457±8	1.00±0.15
3.1.3	31.9±3.1	28.5±1.9	446±7	0.80±0.11
3.1.2	35.0±3.7	29.0±2.1	462±8	0.79±0.13
3.1.1	30.5±3.4	31.4±2.0	443±8	0.92±0.13
4.1.5	35.2±3.2	38.5±2.0	539±8	0.83±0.09
4.1.3	34.3±3.1	33.4±1.8	503±8	0.60±0.20
4.1.2	32.3±3.0	32.2±1.8	473±7	0.68±0.09
4.1.1	33.0±3.1	32.9±1.8	183±8	0.68±0.09

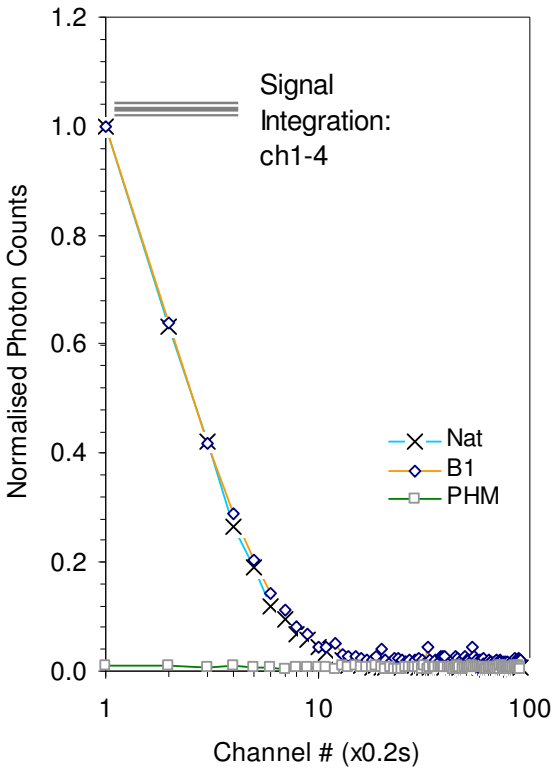

Figure SM4a
OSL decay curves – Normalised intensities (I_N, I_{BG} and $I_{\beta 1}$) measured from a single aliquot of sample 3.1.3 containing about 55 grains, where the subsequent scan showed a dominant single bright quartz grain. The OSL signal was obtained by integrating the first four channels (800 ms) and this interval was also used to define the background signal (PHM). The preheat temperature was 220 °C.

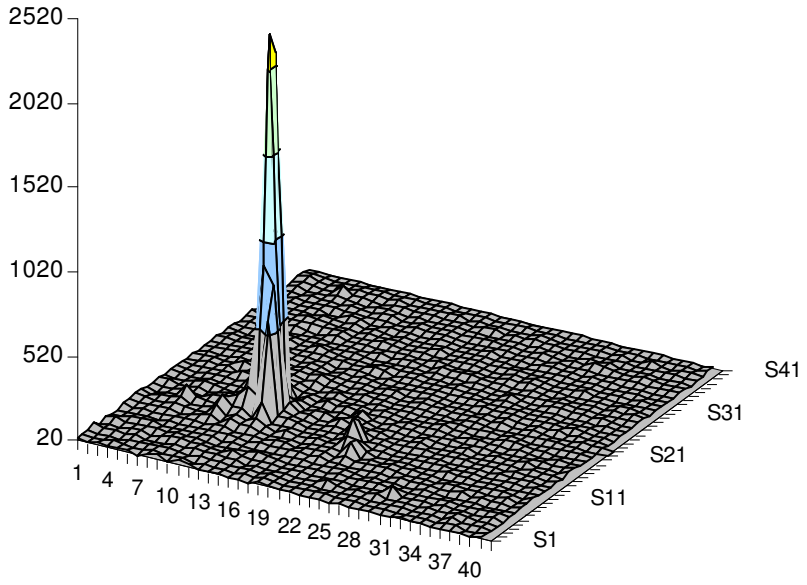

Figure SM4b
Isometric 3D plot of the spatially resolved OSL intensity recorded with an aliquot of sample 3.1.3 containing ~55 quartz grains (200-355 µm) located on the measurement disc. The sharp peak in the plot represents the emission from a single bright grain and for this peak the ratio of signal to background (as shown) was 25. The OSL is recorded at 1600 measurement points within the scanned area (10 x 10 mm); the aliquot had received a laboratory dose of 10 Gy and a 220 ºC preheat before measurement. This disc was categorised has having a dominant individual bright grain.

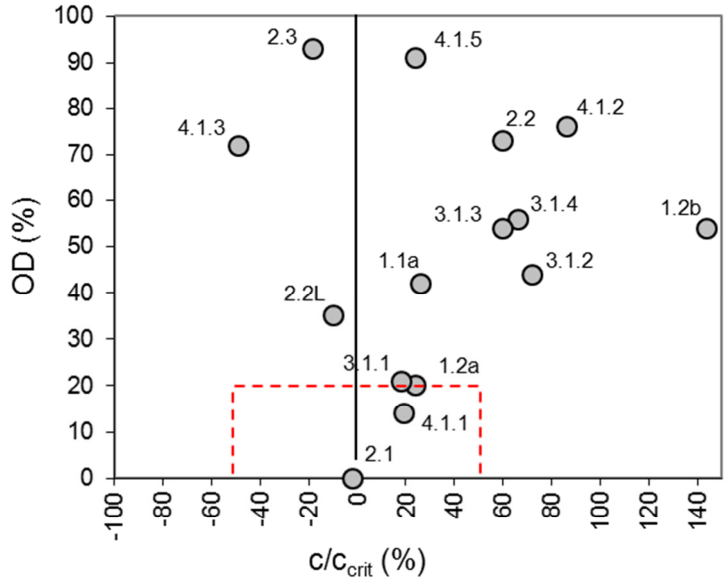

Figure SM4c. Variation in values of overdispersion (σ_b) and skewness (c/c_{crit}) for Bureta samples, where values calculated with results for aliquots containing a dominant individual bright grain (1 gr). The broken line delineates an arbitrary limit of values of 20% OD and ±50% of the critical skewness score (c/c_{crit}), as discussed in the main text.

a) Sample 2.2

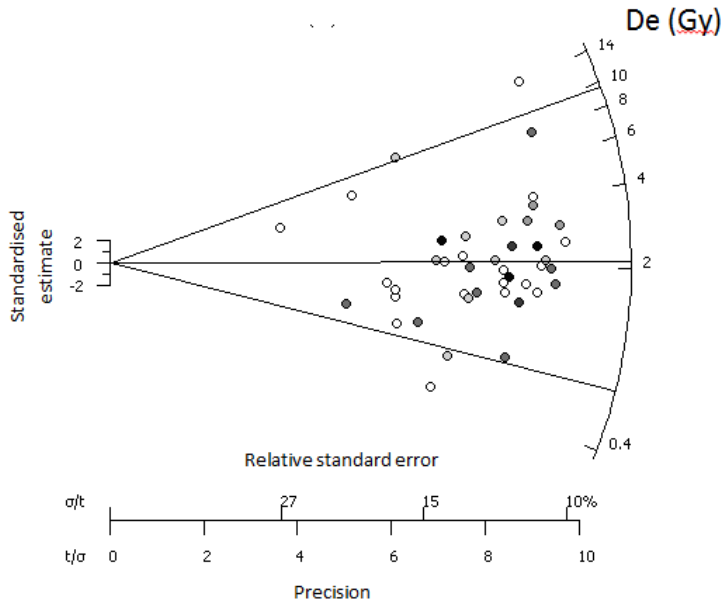

b) Sample 3.1.3

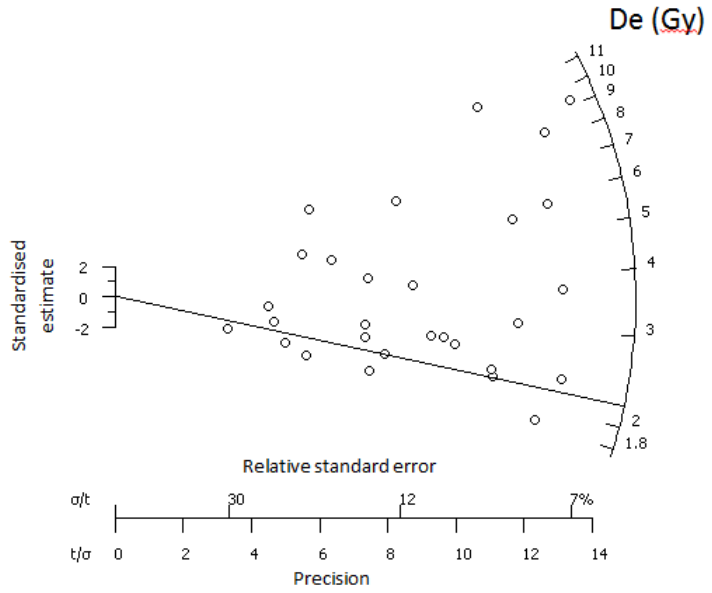

Figure SM4d
Radial graphs for upcast samples a) 2.2 and b) 3.1.3. The graphs (Galbraith 1988) show the values of a standardised D_e estimate plotted against the precision (inverse of the relative standard error) for each aliquot. The dotted line drawn from the origin intersects the radial axis at the average value determined by the statistical model applied: a) sample 2.2, the finite mixture model (FMM) and b) sample 3.1.3, the minimum dose model (MDM). The skewness scores, expressed as a percentage of the critical value, $2\sigma_c$, were 60% for both samples), and the values of overdispersion (OD) were 73% and 54% for samples 2.2 and 3.1.3 respectively (Table SM3). The open symbols represent aliquots containing 1 dominant bright grain and in plot a) for sample 2.2, aliquots containing up to several bright grains are indicated by progressively shaded symbols (count in Table SM3).

4. Additional references

Armitage, S. J., Bailey, R.M., 2005. The measured dependence of laboratory beta dose rates on sample grain size. Radiation Measurements 39, 123-127.
Bailiff, I.K., Mikhailik, V., 2003. Spatially resolved measurement of optically stimulated luminescence and time-resolved luminescence. Radiation Measurements 37, 151-159.
Bailiff, I.K., Tooley, M.J., 2000. Luminescence dating of fine-grain Holocene sediments from a coastal setting. In Holocene land-ocean interaction and environmental change around the North Sea. Shennan, I & Andrews, J Geological Society Special Publications 166: London: Geological Society. 55-67.
Ballarini, M., Wallinga, J., Wintle, A.G., Bos, A.J.J., 2007. A modified SAR protocol for optical dating of individual grains from young quartz samples. Radiation Measurements 42, 360-369.
Barreto, H., Howland, F.M., 2006. Introductory Econometrics, Cambridge University Press, Cambridge, UK.
Cunningham, A.C., Wallinga, J., 2010. Selection of integration time intervals for quartz OSL decay curves. Quaternary Geochronology 5, 657-666.
Galbraith, R.F., 1988. Graphical display of estimates having differing standard errors. Technometrics 30, 395-436.
Galbraith, R.F., 2005. Statistics for Fission Track Analysis. Chapman and Hall/CRC Press, Boca Raton, Florida.
Göksu, H.Y., Bailiff, I.K., Bøtter-Jensen, L., Hütt, G., Stoneham, D., 1995. Inter-laboratory beta source calibration using TL and OSL with natural quartz. Radiation Measurements 24, 479-484.
Li, B., Li, S-H. 2006. Comparison of D_e estimates using the fast component and the medium component of quartz OSL. Radiation Measurements 41, 125-136.
Murray, A.S., Wintle, A.G., 2000. Luminescence dating of quartz using an improved single-aliquot regenerative-dose protocol. Radiation Measurements 32, 57-73.
Prescott, J.R., Hutton, J.T., 1988. Cosmic ray and gamma ray dosimetry for TL and ESR. Radiation Measurements 14, 223-227.
Steffen, D., Preusser, F., Schlunegger, F., 2009. OSL quartz age underestimation due to unstable signal components. Quaternary Geochronology 4, 353-362.